Feasibility study of broad band efficient “water window” source

Takeshi Higashiguchi[1,2], Takamitsu Otsuka[1], Noboru Yugami[1,2], Weihua Jiang[3], Akira Endo[4], Bowen Li[5], Padraig Dunne[5], and Gerry O’Sullivan[5]

[1]Department of Advanced Interdisciplinary Sciences, Center for Optical Research & Education (CORE), and Optical Technology Innovation Center (OpTIC), Utsunomiya University, Yoto 7-1-2, Utsunomiya, Tochigi 321-8585 Japan

[2]Japan Science and Technology Agency, CREST, 4-1-8 Honcho, Kanagawa, Saitama 332-0012 Japan

[3]Department of Electrical Engineering, Nagaoka University of Technology, Kami-tomiokamachi 1603-1, Nagaoka, Niigata 940-2188 Japan

[4]Research Institute for Science and Engineering, Waseda University, Okubo 3-4-1, Shinjuku, Tokyo 169-8555 Japan

[5]School of Physics, University College Dublin, Belfield, Dublin 4, Ireland

Abstract

We demonstrate a table-top broadband emission water window source based on laser-produced high-Z plasmas. Resonance emission from multiply charged ions merges to produce intense unresolved transition arrays in the 2 to 4 nm region, extending below the carbon K edge (4.37 nm). Arrays resulting from $n = 4-4$ transitions are overlaid with $n = 4-5$ emission and shift to shorter wavelength with increasing atomic number. From spectral analysis, a guideline for microscope construction design for single-shot live cell imaging is proposed based on the use of a bismuth plasma source, coupled with multilayer mirror optics.

Development of shorter wavelength sources in the extreme ultraviolet (EUV) and soft x-ray spectral regions has been motivated by their application in a number of high profile areas of science and technology. One such topic is the challenge of three-dimensional imaging and single-shot flash photography of microscopic biological structures, such as cells and macromolecules, *in vivo* [1]. For x-ray microscopy, the x-ray source should emit a sufficient photon flux to expose the image of the biological sample on the detector. The most practical light source of high-power, high-brightness x-rays has been radiation from synchrotrons and more recently from free electron lasers (FEL) [2]. Table-top sources using ethanol sprays and liquid nitrogen droplets are being developed for use with zone plates for transmission microscopy. Recently the λ = 2.48 nm narrowband emission from a liquid-nitrogen-jet laser-plasma [3] was successfully combined with state-of-the-art normal-incidence multilayer condenser optics and 20-nm zone-plate imaging optics to demonstrate laboratory water-window x-ray microscopy [4] with the resolution less than 25 nm and synchrotron-like image quality on biological and soil science samples. In addition development of a high-brightness source based on a focused electron-beam impacting a liquid water jet resulting in 2.36 nm emission has also been reported [5]. The emission energy, however, is quite low when using line emission with low reflectively collector mirrors. As a result, no single-shot flash photographs by use of the laboratory scale source are available to date. To overcome the low efficiency imposed by line sources, we propose using high power water-window emission from laser-produced high-*Z* plasmas, analogous to the scheme used for efficient, high-volume manufacturing EUV sources.

Efficient, high-power extreme-ultraviolet (EUV) sources for semiconductor lithography at 13.5 [6] and 6.7 nm [7-9] based on laser-produced plasmas have been demonstrated in high-

volume manufacturing of integrated circuits (IC) having node sizes of 22 nm or less [10]. Plasmas of the high-Z elements Sn and Gd produce strong resonant emission due to 4d–4f and 4p–4d transitions at 13.5 nm and 6.7 nm, respectively, which overlap in adjacent ion stages to yield an intense unresolved transition array (UTA) in their spectra. The in-band high-energy emission is thus attributable to hundreds of thousands of near-degenerate resonance lines lying within a narrow wavelength range.

Before discussing the high-power water window source, it is important to summarize the characteristics of efficient UTA light sources used in the 5 to 15 nm region. All are based on n = 4–n = 4 (4d–4f and 4p–4d) transitions that overlap to generate an intense UTA. For efficient 13.5-nm operation, which corresponds to a photon energy $h\nu \approx 92$ eV, it is important to produce an optimum plasma electron temperature of 30–50 eV. The rare-earth elements of gadolinium (Gd, Z = 64) and terbium (Tb, Z = 65) produce strong emission near λ = 6.7 nm ($h\nu \approx 183$ eV) which is maximized at electron temperatures in the 100–120 eV range depending on initial focusing conditions [7-9]. The spectral behavior of Gd and Tb plasmas is expected to be largely similar to that of Sn plasmas, because in the temperature range of interest, both are dominated by 4d open-shell ions. Although the conversion efficiency (CE) from the input laser energy to the output in-band EUV emission energy depends on the bandwidth (BW) of the reflection coefficient of the multilayer mirror (MLM), the maximum CEs have been observed to be higher than 1%. Because it moves to shorter wavelength with increasing atomic number, Z, the n = 4–n = 4 UTA is expected to lie in the water window if higher Z elements from Z = 79 (Au) to Z = 83 (Bi) are used [11-13]. Higher Z elements such as uranium also emit in the water window but their radioactivity inhibits their use. Previous work on high-Z plasmas as radiation sources has largely concentrated on the production of

quasicontinuum spectra at low laser intensity [14-16]. According to the numerical evaluation in Fig. 1, the calculated peak wavelengths of the strongest $n = 4–n = 4$ ($4d–4f$) transitions are shifted to shorter wavelength. From this plot it is clear that maximum overlap between emissions from different stages occurs in the lanthanides and corresponds, from an atomic physics viewpoint, to the localization of the $4f$ wavefunction in the ionic core where its overlap with the $4d$ changes little with ion stage. For lower Z elements the emission extends over a broader energy range due to differing degrees of $4f$ localization while the 4d and $4p$ spin orbit splitting causes the emission to diverge to form two or three distinct emission regions at the higher Z end. Our calculations show that high-Z plasmas, at an electron temperature in the range 570 to 600 eV, radiate strongly near 3.9 nm from Bi plasmas [11-13]. At electron temperatures higher than 800 eV, strong UTA emission around 3.2 nm is expected. We have initiated a number of experiments to explore how this emission may be optimized in practice. We focus on the possibility of using the high output energy of the “water window” emission due to the many strong resonance lines that form UTA in a bismuth plasma for single-shot flash imaging as a table-top source. In this letter, we demonstrate an efficient water window source based on strong UTA band emission in laser-produced high-Z plasmas, such as Au, Pb, and Bi. Our proposed procedure for producing the water window emission is expected to be efficient and scalable in output yield.

To evaluate the spectral behavior, two Nd:yttrium-aluminum-garnet (Nd:YAG) lasers operating at 1064 nm produced maximum pulse energies of 200 mJ for a pulse duration of 150 ps (FWHM) and 400 mJ at a pulse duration of 10 ns (FWHM), respectively. The laser was focused perpendicularly onto low-density targets with a 10-cm focal length lens. The maximum focused intensity was approximately 1×10^{14} W/cm^2 at a constant focal spot

diameter of 30 μm (FWHM). The laser was operated in single shot mode. A flat-field grazing incidence spectrometer with 2400 grooves/mm variable line space grating was positioned at 45° with respect to the incident laser axis. Time-integrated spectra were measured by a thermoelectrically cooled back-illuminated x-ray charge coupled device (CCD) camera. The typical spectral resolution was better than 0.005 nm.

Figures 1(a)–1(c) show time-integrated spectra from Au, Pb, and Bi plasmas at a laser intensity of 1×10^{14} W/cm^2 with 150-ps pulse duration. The typical time-integrated EUV spectra between 1 and 6 nm from each element produced strong broadband emission near 4 nm, which was mainly due to $n = 4–n = 4$ transitions from ions with an open 4*f* or 4*d* outermost subshell, together with broadband emission around 2–4 nm due to $n = 4–n = 5$ transitions from multi-charged state ions with an outermost 4*f* subshell. The latter merge to form a structured feature from which the contributing ion stages may be readily inferred. The intensity of the $n = 4–n = 4$ UTA emission is higher than that of the $n = 4–n = 5$ emission. The atomic number spectral dependence is summarized in Fig. 1(d). The predicted photon energy of each experimental peak wavelength was shifted to higher photon energy with increasing atomic number. Neither the emission spectra nor the plasma electron temperatures, however, have been optimized, as shown below. The emission intensity of the $n = 4–n = 5$ transitions, however, was compared with that of the $n = 4–n = 4$ UTAs. The strong emission at 3.15 nm due to the $n = 4–n = 4$ UTA in Bi plasmas may be coupled with a Sc/Cr MLM with a reflection coefficient of 15% [17] and its variation with electron temperature was calculated with Cowan's suite of atomic structure codes in order to predict its evolution with increasing laser flux [18].

Figures 2(a) and 2(b) show the time-integrated Bi spectra and the laser intensity dependence of the peak photon energies of $n = 4-n = 4$ and $n = 4-n = 5$ transitions. The position of the $n = 4-n = 4$ transition peak was observed to be unchanged. The position of the $n = 4-n = 5$ peak, on the other hand, shifts to larger photon energy with increasing laser intensity because of the rise in electron temperature and associated charge states. However, the strong emission expected around 3.2 nm, which originates from the $n = 4-n = 4$ UTA, was not observed in this laser intensity region [11-13].

To explain the Bi spectra, we compare the results of calculation for some experimental temperatures with the experimental spectrum, as shown in Fig. 3(a). In this figure, four regions corresponding to emission peaks are identified. It should be remembered that this spectrum is integrated both spatially and temporally over the duration of the laser pulse. The emission in region 1 results primarily from 4f -5g transitions in ions with an open 4f subshell, that in region 2 and 3 from 4p-4d and 4d-4f transitions ions with an open 4d subshell, the higher energy feature resulting from more highly ionized species while the emission in region 4 is associated mainly with 4d-4f emission from lower stages with an open 4f outmost subshell. Thus the bulk of the emission from regions 1 and 4 are associated with the recombining phase of the expanding plasma plume.

In Figure 3(b) calculated spectra at different electron temperatures higher than 800 eV are presented. Our calculations show that high-Z plasmas, at an electron temperature lower than 700 eV (Fig. 3(a)), radiate strongly near 3.9 nm. However, in the case of higher electron temperatures from 800 to 1500 eV the strongest emission is expected around 3.2 nm, suitable for coupling to Sc/Cr MLMs [17]. Thus for an optimized source, we should produce a

plasma at a higher electron temperature plasma of around 1 keV. To compare with a conventional water window laser-produced plasma line emission source, the relative intensity of the Bi plasma emission in our experiment was compared with 2.48 nm nitrogen line emission from a Si_3N_4 planar target and was observed to be 1.2 times higher within a bandwidth of 0.006 nm (FWHM) [17,19] even though the plasma electron temperature was much lower than the optimum value.

To explore the dependence of the water window emission on laser pulse duration and target composition, we confirmed that use of a low-density target and subnanosecond laser pulse reduces the effects of self-absorption, exactly analogous to the 6.7-nm EUV source plasma behavior [7-9]. In the case irradiation with the 150 ps laser (Fig. 4(a)), the spectral structure was unchanged for different initial Bi densities of 80% (foam target) and 100% (solid target). The intensity, however, increased in the case of the low-density target for ns laser pulse irradiation due to the suppression of self-absorption in the expanding plasma, as shown in Fig. 4(b). From these spectra, we can infer that the average electron temperature in the ns laser-produced Bi plasma is lower than that of the ps laser-produced plasma due to the much different laser intensity attainable at short pulse duration. Thus, an efficient, high-power requires the production of a high-temperature and low-density Bi plasma. However, the intensity needed to achieve the electron temperatures higher than 1 keV required is currently unobtainable with commercially available table-top solid-state lasers.

Taking the experimental and numerical results into account, we now propose a high brightness, high power water window source for single shot imaging at the laboratory scale. Our proposed method has the advantage that the EUV energy efficiency and atomic number

dependence can be scaled based on fundamental properties of the plasma source. The electron temperature, T_e, in a high-Z plasma rises with increasing laser intensity as $T_e \propto (I_L \lambda_L^2)^{0.4}$, where I_L and λ_L are the laser intensity and wavelength, respectively [20]. To produce not only a Bi plasma with a high electron temperature of the order of 1 keV but also one that has low density and is optically thin, we should switch to a CO_2 laser operating at a wavelength of 10.6 μm with a 100-ps laser pulse duration, due to the low critical density of 1×10^{19} cm^{-3} attainable [21], while maintaining a laser intensity of the order of 10^{13} W/cm^2 [22]. In addition, we should use a dot Bi target with a diameter less than 20 μm to generate a microplasma (to fulfill the requirements for high brightness and a point source) as the expected focal spot size will be ~100 μm in the case of the longer wavelength CO_2 laser beam. Since, because of the broad band nature of the emission zone plate components cannot be used, one possible solution would be to use a transmission planar x-ray nano-waveguide to image the sample [23]. To achieve high resolution in the recorded image, we should also switch the recording device from x-ray CCD cameras to sensitive EUV resists to overcome the resolution limitation of the CCD pixel size, coupled with Schwarzschild optics, consisting of Sc/Cr MLMs with a reflection coefficient of the order of 15% around 3.2 nm. Although our proposal is based on a simple microscope construction, the key component is the UTA emitted at 3.2 nm from a hot dense Bi plasma point source, combined with Sc/Cr MLMs and sensitive EUV resists based on photochemical reaction [24,25].

In summary, demonstrated high efficiency emission in the water window spectral region by use of the laser-produced Bi plasmas and have proposed methods to increase it still further. Resonance emission from multiply charged ions merges to produce intense UTA, extending to wavelengths below the carbon K edge. The overall spectral behavior could be

inferred well from simulation. The experimental results also provide a guideline for the design concept for single-shot cell imaging with a novel microscope optical system. The method presented here opens the way for applications in next-generation biological science.

Part of this work was performed under the auspices of MEXT (Ministry of Education, Culture, Science and Technology, Japan) and “Utsunomiya University Distinguished Research Projects.” One of the authors (T.H.) also acknowledges support from The Canon Foundation. The UCD group acknowledges support from Science Foundation Ireland under Principal Investigator Research Grant No. 07/IN.1/1771.

References

[1] J. C. Solem and G. C. Baldwin, Science **218**, 229 (1982).

[2] T. Gorniak, R. Heine, A. P. Mancuso, F. Staier, C. Christophis, M. E. Pettitt, A. Sakdinawat, R. Treusch, N. Guerassimova, J. Feldhaus, C. Gutt, G. Grübel, S. Eisebitt, A. Beyer, A. Gölzhäuser, E. Weckert, M. Grunze, I. A. Vartanyants, and A. Rosenhahn, Opt. Exp. **19**, 11059 (2011).

[3] P. A. C. Jansson, U. Vogt, and H. M. Hertz, Rev. Sci. Instrum. **76**, 043503 (2005).

[4] P. A. C. Takman, H. Stollberg, G. A. Johansson, A. Holmberg, M. Lindblom, and H. M. Hertz, J. Microsc. **226**, 175 (2007).

[5] P. Skoglund, U. Lundström, U. Vogt, and H. M. Hertz, Appl. Phys. Lett. **96**, 084103 (2010).

[6] *EUV Sources for Lithography*, edited by V. Bakshi (SPIE, Bellingham, WA, 2005).

[7] T. Otsuka, D. Kilbane, J. White, T. Higashiguchi, N. Yugami, T. Yatagai, W. Jiang, A. Endo, P. Dunne, and G. O'Sullivan, Appl. Phys. Lett. **97**, 111503 (2010).

[8] T. Otsuka, D. Kilbane, T. Higashiguchi, N. Yugami, T. Yatagai, W. Jiang, A. Endo, P. Dunne, and G. O'Sullivan, Appl. Phys. Lett. **97**, 231503 (2010).

[9] T. Higashiguchi, T. Otsuka, N. Yugami, W. Jiang, A. Endo, B. Li, D. Kilbane, P. Dunne, and G. O'Sullivan, Appl. Phys. Lett. **99**, 191502 (2011).

[10] C. Wagner and N. Harned, Nat. Photonics **4**, 24 (2010).

[11] D. Kilbane, J. Phys. B: At. Mol. Opt. Phys. **44**, 165006 (2011).

[12] B. Li, A. Endo, T. Otsuka, C. O'Gorman, T. Cummins, T. Donnelly, D. Kilbane, W. Jiang, T. Higashiguchi, N. Yugami, P. Dunne, G. O'Sullivan, Proc. SPIE **8139**, 81390P (2011).

[13] T. Higashiguchi, T. Otsuka, N. Yugami, W. Jiang, A. Endo, P. Dunne, B. Li, and G. O'Sullivan, SPIE Newsroom DOI: 10.1117/2.1201109.003765 (2011).

[14] P. K. Carroll and G. O'Sullivan, Phys. Rev. A **25**, 275 (1982).

[15] G.-M. Zeng, M. Takahashi, H. Daido, T. Kanabe, H. Aritome, M. Nakatsuka, and S. Nakai, J. Appl. Phys. **67**, 3597 (1990).

[16] G.-M. Zeng, H. Daido, T. Togawa, M. Nakatsuka, S. Nakai, and H. Aritome, J. Appl. Phys. **69**, 7460 (1991).

[17] Y. Uspenskii, D. Burenkov, T. Hatano, and M. Yamamoto, Opt. Rev. **14**, 64 (2007).

[18] R. D. Cowan, *The Theory of Atomic Structure and Spectra*, University of California Press, Berkeley (1981).

[19] M. Bertilson, O. von Hofsten, U. Vogt, A. Holmberg, and H. M. Hertz, Opt. Exp. **17**, 11057 (2009).

[20] D. Colombant and G. F. Tonon, J. Appl. Phys. **44**, 3524 (1973).

[21] H. Tanaka, A. Matsumoto, K. Akinaga, A. Takahashi, and T. Okada, Appl. Phys. Lett. **87**, 041503 (2005).

[22] Y. Ueno, T. Ariga, G. Soumagne, T. Higashiguchi, S. Kubodera, I. Pogorelsky, I. Pavlishin, D. Stolyarov, M. Babzien, K. Kusche, and V. Yakimenko, Appl. Phys. Lett. **90**, 191503 (2007).

[23] S. P. Kruger, K. Giewekemeyer, S. Kalbfleisch, M. Bartels, H. Neubauer, and T. Salditt, Opt. Exp. **18**, 13492 (2010).

[24] T. Gowa, N. Fukutake, Y. Hama, K. Hizume, T. Kashino, S. Kashiwagi, R. Kuroda, A. Masuda, A. Oshima, T. Saito, K. Sakaue, K. Shinohara, T. Takahashi, T. Urakawa, K. Ushida, and M. Washio, J. Photopolym. Sci. Technol. **22**, 273 (2009).

[25] T. Gowa, T. Takahashi, A. Oshima, S. Tagawa, and M. Washio, Radiat. Phys. Chem. **80**, 248 (2011).

FIGURE CAPTIONS

Fig. 1 Time-integrated spectra from the picosecond-laser-produced high-*Z* plasmas by use of Au (a), Pb (b), and Bi (c), respectively, and the atomic number dependence on the photon energies of peak emission of the $n = 4–n = 4$ transition (circles) and the $n = 4–n = 5$ transition (rectangles).

Fig. 2 Spectral behaviors of the Bi plasmas in the laser intensity dependence on the observed emission spectra (a), the peak wavelength of of the $n = 4–n = 4$ transition (circles) and the $n = 4–n = 5$ transition (rectangles) (b).

Fig. 3 ***The numerically calculated spectra at low (a) and high (b) electron temperatures, respectively.***

Fig. 4 Spectral comparison with the laser pulse duration of ps (a) and ns (b) at the initial densities of 100% (bold) and 80% (fine), respectively.

Fig. 1

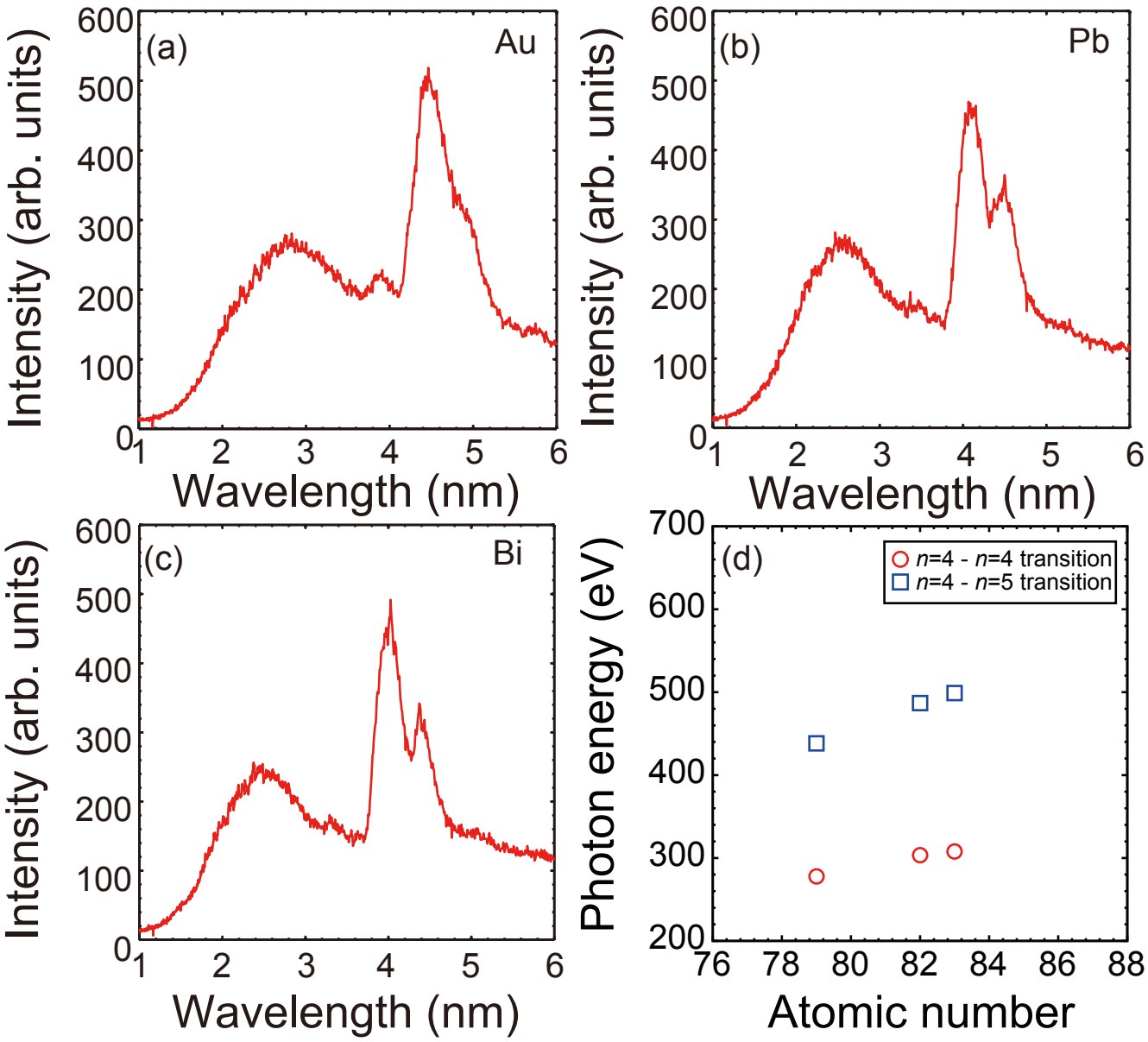
(a)
Au
(b)
Pb
(c)
Bi
(d)
Intensity (arb. units)
Wavelength (nm)
Photon energy (eV)
Atomic number
n=4 - n=4 transition
n=4 - n=5 transition

Fig. 2

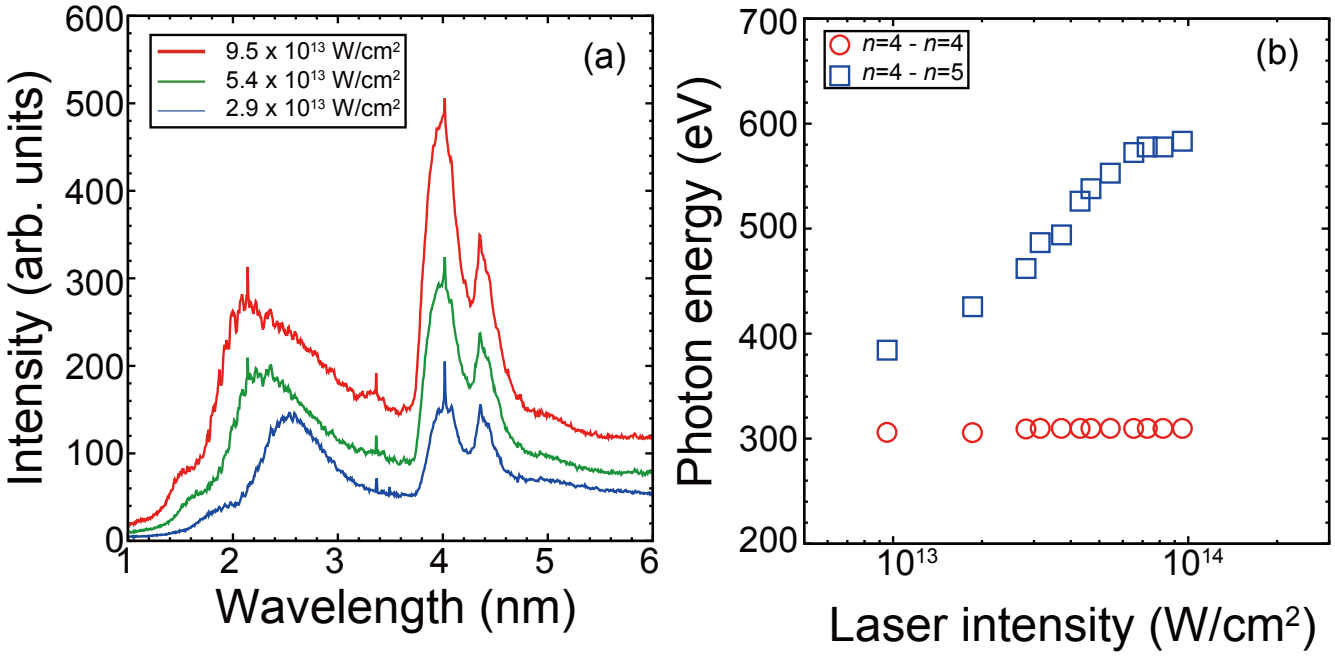
9.5 x 10¹³ W/cm²
5.4 x 10¹³ W/cm²
2.9 x 10¹³ W/cm²
(a)
Intensity (arb. units)
Wavelength (nm)
n=4 - n=4
n=4 - n=5
(b)
Photon energy (eV)
Laser intensity (W/cm²)

Fig. 3 (from Bowen and Taka)

Fig. 4

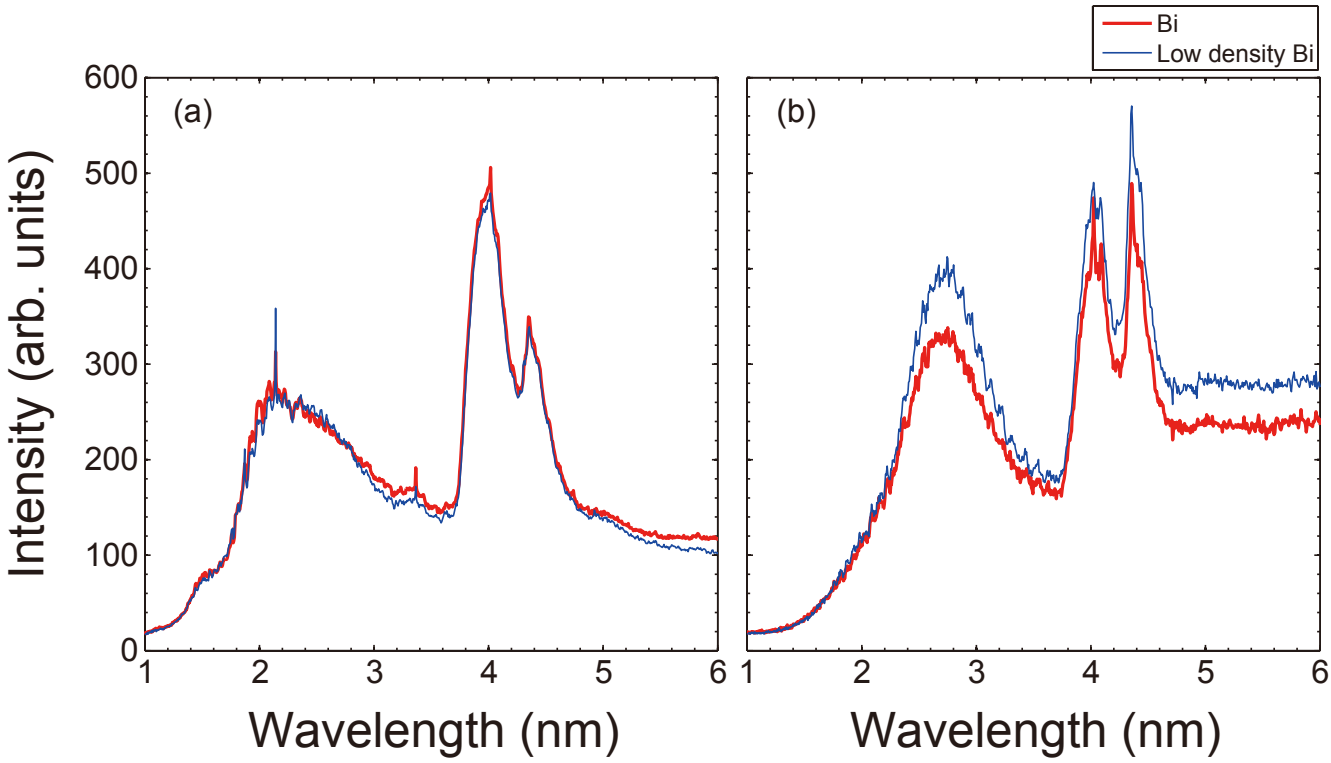
Bi
Low density Bi
(a)
(b)
Intensity (arb. units)
0
100
200
300
400
500
600
1
2
3
4
5
6
Wavelength (nm)
Wavelength (nm)